Environmental Science Nano

ROYAL SOCIETY OF CHEMISTRY

PAPER

View Article Online
View Journal | View Issue

Cite this: *Environ. Sci.: Nano*, 2020, 7, 2010

Modeling performance of rhamnolipid-coated engineered magnetite nanoparticles for U(VI) sorption and separation†

Neha Sharma, [a] Anushree Ghosh,[a] John D. Fortner*[b] and Daniel E. Giammar *[a]

Based on tunable properties, engineered nanoparticles (NPs) hold significant promise for water treatment technologies. Motivated by concerns regarding toxicity and non-biodegradability of some nanoparticles, we explored engineered magnetite (Fe_3O_4) nanoparticles with a biocompatible coating. These were prepared with a coating of rhamnolipid, a biosurfactant primarily obtained from *Pseudomonas aeruginosa*. By optimizing synthesis and phase transfer conditions, particles were observed to be monodispersed and stable in water under environmentally relevant pH and ionic strength values. These materials were evaluated for U(VI) removal from water at varying dissolved inorganic carbon and pH conditions. The rhamnolipid-coated iron oxide nanoparticles (IONPs) showed high sorption capacities at pH 6 and pH 8 in both carbonate-free systems and systems in equilibrium with atmospheric CO_2. Equilibrium sorption behavior was interpreted using surface complexation modeling (SCM). Two models (diffuse double layer and non-electrostatic) were evaluated for their ability to account for U(VI) binding to the carboxyl groups of the rhamnolipid coating as a function of the pH, total U(VI) loading, and dissolved inorganic carbon concentration. The diffuse double layer model provided the best simulation of the adsorption data and was sensitive to U(VI) loadings as it accounted for the change in the surface charge associated with U(VI) adsorption.

Received 22nd April 2020,
Accepted 11th June 2020

DOI: 10.1039/d0en00416b

rsc.li/es-nano

Environmental significance

The current study provides evidence that biosurfactants can be effectively used to coat and stabilize iron oxide nanoparticles in aqueous suspension. Biosurfactants such as rhamnolipids are biodegradable, and their use raises fewer environmental concerns than the use of their synthetic counterparts. Due to their stability under environmentally relevant pH and ionic strength conditions, these engineered materials can be successfully implemented in water treatment systems for the removal of potent contaminants without causing any further downstream pollution. Rhamnolipid-coated iron oxide nanoparticles were demonstrated to be able to adsorb the environmentally significant contaminant U(VI), and the effects of water chemistry on adsorption were successfully modeled within a reaction-based surface complexation modeling framework.

Introduction

Uranium can be introduced into aquatic systems *via* a number of anthropogenic pathways, including discharge from mining and milling operations, leading to public health concerns.[1] Considering chronic health effects associated with uranium, the current U.S. EPA maximum contaminant level (MCL) for uranium in drinking water is 30 μg L^{-1}. Uranium predominantly exists at oxidation states of +IV and +VI, U(VI) being the more mobile form and the dominant one present under oxidizing conditions.[2] The fate of U(VI) in aquatic environments strongly depends on the pH, redox potential, presence of divalent cations and dissolved inorganic carbon.[2] Processes involving redox, dissolution–precipitation and adsorption–desorption reactions underpin uranium mobility in natural and engineered systems.[3]

Strategies for removal of uranium under oxidizing conditions often rely on adsorption processes. Recently, a variety of nanomaterial adsorbents, including aluminium oxides, iron oxides, titanium oxides and graphene oxides have been developed and evaluated for their efficacy towards uranium removal from water systems.[4–15] Iron oxide nanoparticles (IONPs) are one of the promising materials for

[a] *Department of Energy, Environmental and Chemical Engineering, Washington University in St. Louis, St. Louis, Missouri 63130, USA.*
E-mail: giammar@wustl.edu; Tel: +1 (314) 935 6849
[b] *Department of Chemical and Environmental Engineering, Yale University, New Haven, Connecticut 06520, USA*

† Electronic supplementary information (ESI) available: Phase transfer efficiency obtained for different parameters, aqueous reactions considered in the surface complexation model, calculations for estimating the number of rhamnolipids attached per nanocrystal, the variation of UO_2^{2+} under different pH and carbonate conditions, speciation of U(VI) under different pH and carbonate conditions, NEM parameter fitting to adsorption isotherms and effect of U(VI) loading on zeta potential of nanoparticles. See DOI: 10.1039/d0en00416b

the removal of contaminants from water systems due to their large specific surface area, tunable surface chemistries and potential biocompatibility.[4,7,16,17] A number of studies have focused on the use of magnetite nanoparticles for contaminant removal due to their unique magnetic properties which allow easy removal and collection from water systems by application of an external magnetic field.[6,11,13,16–19]

Synthesis of water-dispersible IONPs has been achieved by chemical co-precipitation, microemulsion and hydrothermal routes.[17] These methods produce poorly crystalline and aggregated nanoparticles. This has encouraged the use of non-hydrolytic routes (organic phase synthesis) for the synthesis of IONPs, allowing for reproducible and highly crystalline nanostructures with uniform size and shape.[16,17,20] Typically, nanoparticles obtained from these routes are stable in nonpolar solvents and are capped with nonpolar moieties (*e.g.* oleic acid) to lower surface energies and prevent aggregation.[16,17,20] Surface coatings reduce particle aggregation as they counter the attractive interparticle forces with repulsive steric or electrostatic forces.[21]

For successful application of IONPs dispersed in nonpolar solvents to water treatment, the outer hydrophobic coating needs to be modified to be hydrophilic.[16] Ligand exchange and ligand addition methods are used for surface modification of as-synthesized IONPs.[16,20] In the ligand exchange method, the original coating is replaced by the desired amphiphile or surfactant that has an affinity for both the nanoparticle surface and the water interface. In the case of ligand addition, a hydrophobic tail of the selected amphiphile interacts with the original coating while the hydrophilic tail is oriented towards the water, yielding a stable aqueous suspension of the nanoparticles.[16,22] Various synthetic organic surface coatings, including oleic acid, humic acid, stearic acid and polymers,[6,18,22–25] have been explored for stabilization of IONPs synthesized through non-hydrolytic routes. These stabilized IONPs have shown tremendous potential in the removal of metals and metalloids from water.[9,14,19,26] However, these coatings are often toxic or non-biodegradable, and they may pose environmental risks if the particles are not retained in the treatment unit. Recent studies have explored naturally derived coatings and biosurfactants for the stabilization of the nanoparticles.[5,27–31] The addition of micro-algal exudate as a biosurfactant in the preparation of polyethylene nanoparticles reduced their aggregation in the salt solutions.[32] The performance of nanoparticles for contaminant removal can also be significantly improved by the addition of naturally-derived coatings.[5,33] The use of chitosan in a nanocomposite with graphene oxide enhanced the sorption capacity for U(VI) removal.[33,34] Cyclodextrin-modified maghemite nanocomposites showed remarkable stability as no change in their efficiency for U(VI) removal was observed even after four cycles of adsorption/desorption.[6]

Biosurfactants are amphiphilic molecules produced by microorganisms to reduce interfacial tension in the process of utilization of various substrates. As compared to their synthetic counterparts, biosurfactants are typically less toxic and more biodegradable.[35,36] An emerging application of biosurfactants is in the stabilization of nanomaterials as they reduce the surface energy at the interface and prevent aggregation of nanoparticles.[37] Rhamnolipids are glycolipids (biosurfactants) produced primarily by *Pseudomonas aeruginosa* at relatively high concentrations extracellularly, and they consist of a rhamnose moiety and a 3-(hydroxyalkanoyloxy) alkanoic acid fatty acid tail.[29] Recent studies show that rhamnolipids act as an effective stabilizer for palladium-coated nanoscale zero-valent iron (nZVI) nanoparticles and prevent their aggregation.[21,30,38] Another study observed that the inclusion of rhamnolipid in the synthesis of chitosan nanoparticles improved their stability and monodispersity.[31] Rhamnolipids also enhanced soil deliverability and reactivity of nZVI for *in situ* remediation.[39] Rhamnolipids have also been used as capping agents in several studies for the synthesis of stabilized nanoparticles.[27,28,31,40–42] However, the potential of rhamnolipids to stabilize magnetite nanoparticles had not previously been observed; consequently, the use of rhamnolipid-coated IONPs as adsorbents for metals is also unexplored.

Surface complexation modeling (SCM) is a robust approach to model the partitioning of sorbates between solid and solution phases as a function of pH, solute concentration, and ionic strength. The prediction of U(VI) adsorption on sorbents is confounded by complexities of U(VI) speciation under different dissolved inorganic carbon conditions.[2,3,43] In carbonate-containing systems, U(VI) adsorption to sorbents is affected by the formation of stable soluble U(VI)–CO_3 complexes at higher pH values.[3,8,43] SCM has been previously applied to engineered nanomaterials to model sorption of U(VI) over a wide pH range and different carbonate conditions.[8,14,44–47] As model parameters will be different for different adsorbents, we aimed to understand if SCM could interpret metal binding to IONPs coated with rhamnolipid. The model can also yield insight into the mechanism of U(VI) binding onto these rhamnolipid-coated IONPs.

In this work, we have explored rhamnolipids as potential biocompatible ligands for stabilizing superparamagnetic magnetite nanoparticles in water. The efficiency of this coating was then evaluated by using rhamnolipid-coated nanoparticles for U(VI) sorption under varying conditions of pH and dissolved inorganic carbon (DIC). The three primary objectives of the study were to (i) optimize conditions for coating as-synthesized magnetite nanoparticles with rhamnolipids for stabilizing them in water suspensions, (ii) evaluate the performance of rhamnolipid-coated IONPs for U(VI) adsorption under varying conditions of pH and carbonate, and (iii) develop a surface complexation model to

interpret U(VI) adsorption performance onto these engineered nanoparticles.

1. Experimental section

1.1. Materials and methods

Iron(III) oxide (hydrated, catalyst grade, 30–50 mesh), oleic acid (technical grade, 90%), 1-octadecene (technical grade, 90%), sodium chloride (ACS reagent, 99.0%), magnesium chloride hexahydrate (ACS reagent, 99%), sodium hydroxide (ACS reagent 99.0%), sodium bicarbonate (ACS reagent 99.0%), sodium carbonate (ACS reagent 99.0%) and nitric acid (trace metal grade) were purchased from Sigma-Aldrich. Hexane, acetone and ethanol were also purchased from Sigma-Aldrich and were used without purification. Rhamnolipid (90%) standard was purchased from AGAE Technologies. A U(VI) stock solution was prepared from uranyl nitrate ($UO_2(NO_3)_2{\cdot}6H_2O$).

1.2. Nanoparticle synthesis process and phase transfer

Monodispersed IONPs (~8 nm) were synthesized using a published method.[20,22] Briefly FeOOH powder (0.178 g, finely ground), oleic acid (2.26 g) and 1-octadecene (5.0 g) were thermally decomposed at 320 °C to form brown-black colloids that were further purified using acetone and hexane to obtain 8 nm IONPs dispersible in apolar solvents. Purified IONPs were collected in hexane and stored in the dark at room temperature. To make the IONPs suitable for water treatment applications, these were phase transferred from hexane to water by a bilayer ligand addition method using a probe sonicator. For optimizing phase-transfer conditions, varying amounts of IONPs and rhamnolipids were used. Specifically, IONPs in hexane (400–800 μL) were combined with 8 mL of rhamnolipids (60–100 mg L^{-1}) in aqueous solution combined in a 20 mL glass vial and probe sonicated (UP 50H, Dr. Hielscher, GMHB) under different conditions of time and amplitude (details in ESI,† Table S1). The suspension was kept in a fume hood for 24 hours to remove residual hexane. Unstable particles were removed from the aqueous phase by centrifugation, stirred cell filtration (ultrafiltration cellulose membranes, 100 kDa MWCO), and filtration through a 0.22 μm membrane filter. The optimum parameters were selected based on phase transfer efficiency and hydrodynamic diameter (details in ESI,† Table S1). A stock suspension of IONPs coated with rhamnolipids was then prepared using optimized parameters.

1.3. Characterization of IONPs

IONPs core sizes before and after phase transfer were determined using transmission electron microscopy (TEM, FEI Tecnai G2 Spirit) operated at 120 kV. Sample preparation was done by placing 20 μL of diluted IONP suspension on a carbon-coated copper grid. After drying the grid at room temperature, the images were observed using TEM. The average diameter of the suspended particles was calculated by counting 2000 randomly chosen IONPs from the TEM micrographs using ImageJ software (National Institutes of Health). The phase transfer efficiency was estimated by analyzing dissolved Fe concentrations before and after phase transfer with inductively coupled plasma optical emission spectroscopy (ICP-OES, Perkin Elmer ELAN DRC). Suspensions were prepared for ICP-OES analysis by digesting IONPs suspensions in 10% nitric acid on a hot plate at 100 °C.

The number of rhamnolipid molecules attached per nanoparticle was estimated using the total organic carbon (TOC) content in the aqueous suspension before and after ultracentrifugation.[26] TOC analysis was performed using a total organic carbon analyzer (TOC-L, Shimadzu Scientific Instrument, Inc., MD; 680 °C). The hydrodynamic diameter and zeta potential of IONPs in the aqueous phase were estimated using dynamic light scattering (Zetasizer, Malvern Nano ZS, UK). For both measurements, pH was varied from 4–11 to determine the stability of aqueous suspension over the desired range. The mean value and standard deviation for hydrodynamic diameter and zeta potential were based on triplicate samples and at least 10 readings for each sample. The aggregation kinetics of IONPs in aqueous suspension were determined using time-resolved DLS in the presence of NaCl and $MgCl_2$ over a range of concentrations. All the measurements were done at pH 7.5 ± 0.1 and in accordance with a previously reported procedure.[22] The attachment efficiency (α) for IONPs was calculated by the following equation:[48]

$$\alpha = \frac{k}{k_{\text{fast}}} \tag{1}$$

where k is the initial aggregation rate constant at an examined condition and k_{fast} is the aggregation rate constant under diffusion-limited (fast) aggregation conditions. Slow aggregation occurs at lower salt concentrations due to a repulsive energy barrier, and an increase in salt concentration in this regime generally results in an increase in aggregation rate.[21,48] The minimum salt concentration beyond which there is no effect on aggregation rate is called the critical coagulation concentration (CCC), and k_{fast} is the aggregation rate constant above this point.[21,30,48]

1.4. U(VI) sorption studies

Adsorption edges. Sorption efficiency of rhamnolipid-coated engineered magnetite nanoparticles was evaluated at different pH values (5.5–11.5) at two fixed U(VI) loadings and under three different carbonate conditions (open to atmosphere, carbonate-free system and 1 mM fixed DIC system). U(VI) loadings of 1 μM and 10 μM were selected based on preliminary calculations in MINEQL+ V5.0 that identified conditions that would avoid any possible precipitation of U(VI). For open to atmosphere adsorption experiments, ultrapure water was adjusted to target pH values (5.5–11.5) by 0.1 M HNO_3 and 0.1 M NaOH and continuously

stirred to attain equilibrium with atmospheric CO_2. For achieving equilibrium at higher pH values (>9), predetermined amounts of sodium carbonate and sodium bicarbonate were added to obtain a DIC concentration closer to the value that would be achieved once equilibrium with atmospheric CO_2 was reached at the desired pH.[14] Carbonate-free experiments were performed in a glove box (Coy Laboratory Products Inc., MI) under an N_2 atmosphere where the gas in the glove box was bubbled through a concentrated NaOH solution to remove any traces of CO_2. For adsorption experiments with 1 mM fixed DIC, the amount of acid/base required at desired experimental conditions (pH and U(VI) loading) was predetermined to minimize the contact with the atmosphere.

Adsorption isotherms. The sorption capacity of rhamnolipid-coated nanoparticles was explored at pH 6 and 8 under open to atmosphere and carbonate-free conditions. Two different pH values (6 and 8) were selected as the speciation of U(VI) at the selected pH values varies significantly. For open to atmosphere system, at pH 6, UO_2CO_3 and $(UO_2)_2CO_3(OH)_3^-$ dominate, whereas at pH 8, $UO_2(CO_3)_3^{4-}$, $UO_2(CO_3)_2^{2-}$ and $(UO_2)_2CO_3(OH)_3^-$ are in the majority. However, in carbonate free system, UO_2OH^+ and $(UO_2)_3(OH)_5^+$ exist in the majority at pH 6 whereas $(UO_2)_3(OH)_5^+$, $UO_2(OH)_3^-$ and $(UO_2)_3(OH)_7^-$ dominate at pH 8. U(VI) loading was varied between 0.1 μM and 25 μM at selected carbonate conditions and equilibrated for 24 hours.

For each set of U(VI) adsorption experiments, the suspensions were continuously mixed by end-overend rotation for 24 hours, and the pH was readjusted after 4, 8 and 12 hours. Control experiments without nanoparticles were conducted to monitor any loss of U(VI) throughout the procedure. Similarly, control experiments with only nanoparticles were performed to observe the stability of IONPs at desired pH values. The suspensions from each set of conditions were ultracentrifuged (Sorvall WX Ultra 80, Thermo scientific, T1270) at 40 000 rpm for 2 hours to separate IONPs, and the supernatant was collected for uranium (U) analysis (ICP-MS, PerkinElmer). The concentration of Fe in the supernatant was also measured to monitor the leaching of iron from nanoparticles due to U(VI) adsorption.

1.5. Surface complexation modelling (SCM)

SCM was used to describe sorption of U(VI) to rhamnolipid-coated IONPS over a wide range of pH at three different carbonate conditions and with two different U(VI) initial loadings. The carboxyl group on the rhamnolipid was considered as the main site for UO_2^{2+} sorption. Similar to aqueous complexation, surface complexation reactions predict sorption on the basis of equilibrium complexation of a metal and surface-associated functional groups.[49] The diffuse layer model (DLM) and non-electrostatic model (NEM) were selected to evaluate the impact of pH, DIC and initial U(VI) loadings on the sorption of U(VI) onto rhamnolipid coated IONPs. NEM does not consider electrostatic interactions and simulates surface complexation reactions in a similar way as the corresponding aqueous complexation reactions, however, DLM considers both electrostatic and chemical contributions to adsorption. Before fitting the models to adsorption edge and adsorption isotherm data, surface characteristics (specific surface area, site density and surface acidity constant) of the IONPs were estimated. Potentiometric titration was performed using 30 mg L^{-1} of IONPs suspension, and the data were fitted using NEM and DLM models by varying the surface acidity constant, specific surface area and site density. The best fit was obtained by minimizing the residual sum of squares between experimental and modeled data. The optimized parameters were used in DLM and NEM models to fit the adsorption edge and adsorption isotherm data. The optimal fits for both the models were obtained by varying the $\log K$ values of surface reactions using MINEQL+ V5.0 (Environmental Research Software) and MINFIT.[50] The full set of aqueous reactions (details in ESI†) along with the U(VI) surface complexation reactions were considered.

2. Results and discussion

2.1. Synthesis and characterization of rhamnolipid-coated nanoparticles

Nanoparticles obtained after the thermal decomposition method were highly uniform, spherical and had an average size of 9.0 ± 0.8 nm as shown in TEM micrographs (Fig. 1a). XRD patterns identified the crystal structure to be face centered cubic (FCC), as expected for Fe_3O_4, which is a spinel ferrite.[9,20] Single domain Fe_3O_4 of this size also displays superparamagnetic characteristics at room temperature, which allows for low energy separation from the aqueous phase by applying a magnetic field.[9,20]

As particles were synthesized through a nonhydrolytic route using oleic acid as a capping agent; they were only stable in nonpolar solvents and required a passivating layer for water transfer. For this, a mixture of monorhamnolipid and dirhamnolipid was employed. The hydrophobic tail of oleic acid associates with the hydrophobic tail of the rhamnolipid (*via* hydrophobic and dispersive van der Waals forces), and the hydrophilic tail of the rhamnolipid (possessing carboxylic groups) interacts with water molecules to render IONPs stable in water systems.[19] The details of the conditions considered for optimizing phase transfer conditions are shown in ESI† (Table S1). The sonication amplitude used for phase transfer ranged between 80% and 100%. The phase transfer efficiency decreased significantly when the amplitude was less than 80% (Table S1†). The average time required for efficient phase transfer was 10–12 minutes, and IONPs volume was varied from 400 μL to 600 μL (2.2–3.3 mg as Fe). Hydrodynamic diameter of 27.6 nm obtained from DLS measurements shows that rhamnolipid forms a thin coating around the nanoparticles at a concentration of 100 mg L^{-1}. Maximum phase transfer

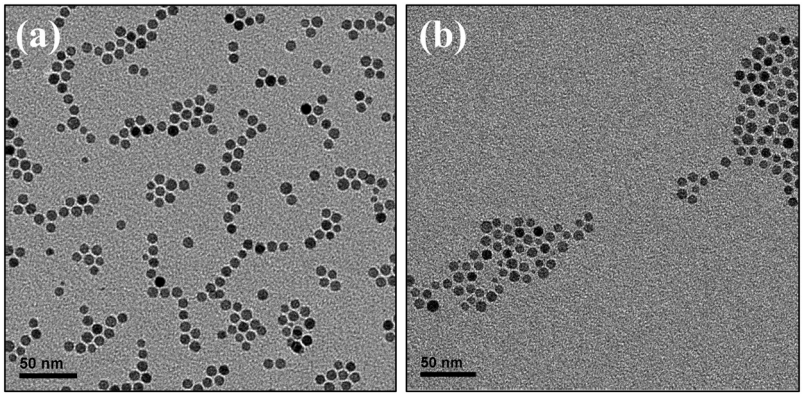

Fig. 1 Transmission electron micrographs for (a) oleic acid-coated nanoparticles in hexane (b) rhamnolipid (bilayer) stabilized nanoparticles in water. Scale bars are 50 nm.

efficiency of 91% was achieved by taking 600 μL of IONPs and 100 mg L^{-1} of rhamnolipid. The yield is higher than other optimized coatings (for similar materials), including oleic acid (70%), dodecyl trimethylammonium bromide (47%), sodium dodecyl benzenesulfonate (68%) and sodium dodecyl sulfate (79%).[22] TEM micrographs (Fig. 1b) confirmed that at the selected conditions, rhamnolipid did not alter the monodispersity and core size of IONPs.

The hydrodynamic diameter of IONPs in the stock suspension used for sorption studies was 27.6 ± 3.4 nm. Zeta potential measurements (Fig. 2a) found that the coated IONPs were negatively charged at pH above 5.5, which is consistent with the pK_a value (4.5–5.5) of rhamnolipids.[51] No significant change in hydrodynamic diameter was observed with the change in pH >5.5, whereas at pH <5.5, destabilization followed by aggregation of nanoparticles was observed. All the experiments described (characterization and sorption) were conducted at pH >5.5. Aggregation kinetics of IONPs were studied to understand the response of nanoparticle suspensions to salt (NaCl and $MgCl_2$) addition (Fig. 3). The aggregation increased with increasing salt concentration until the aggregation rate reached the diffusion-limited regime (α = 1). The critical coagulation concentration was obtained when the attachment efficiency reached unity. The CCC values for rhamnolipid-coated NPs were found to be 62.5 mM and 3 mM for NaCl and $MgCl_2$, respectively. The stability of the suspension can be attributed to the hydrophobic interactions between the first and second layer coatings and steric stabilization induced by rhamnolipid moieties.[21,22,27,28] The CCC values of rhamnolipid-coated IONPs were close to the CCC values obtained using synthetic anionic surfactants with shorter carbon chain lengths (decanoic acid and lauric acid) and containing complex functionalities (sodium dodecyl sulfate and sodium dodecyl benzenesulfonate).[22]

From TOC analysis, the total amount of carbon attached to the nanoparticles was obtained. The number of rhamnolipids attached per nanoparticle was estimated by assuming that one molecule of rhamnolipid attaches to two molecules of oleic acid. From previous studies, it has been shown that the IONPs obtained through thermal decomposition method are in the form of magnetite.[9,52] Assuming a density of 5 g cm^{-3} (for magnetite) and average diameter of 9 nm, it was estimated that 186 rhamnolipid molecules are attached to one nanoparticle upon phase transfer, thus providing a site density of 0.73 sites per nm^2. The calculations are provided in detail in the ESI.†

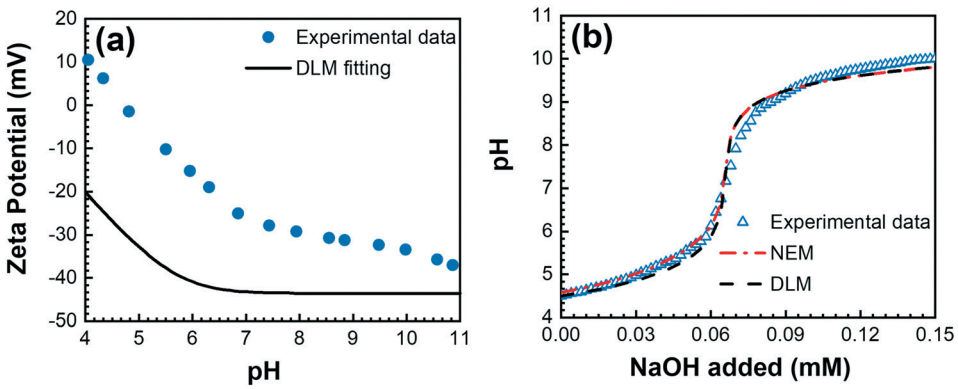

Fig. 2 (a) Zeta potential of rhamnolipid-stabilized IONPs as a function of pH at a nanoparticle concentration of 30 mg L^{-1} and (b) titration curves for rhamnolipid-coated nanoparticle suspensions.

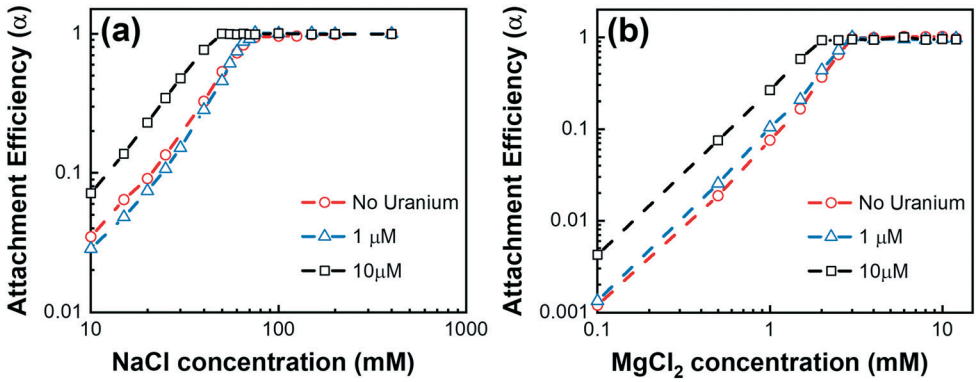

Fig. 3 Effect of U(VI) loading (1 μM and 10 μM) on CCC evaluated using (a) NaCl and (b) $MgCl_2$. The experiment was performed at pH = 7.5 and nanoparticle concentration of 30 mg L^{-1}.

To understand the effect of U(VI) loading on the stability of IONPs, aggregation kinetics in the presence of U(VI) (1 μM and 10 μM) were studied. There was no effect on CCC values when U(VI) loading was 1 μM, whereas the CCC value reduced to 50 mM and 2 mM in presence of NaCl and $MgCl_2$, respectively, when loading was increased to 10 μM (Fig. 3). The aggregation of nanoparticles was likely promoted by adsorption of UO_2^{2+}, which resulted in the reduction of the effective surface charge of IONPs. This can be observed from zeta potential measurements (Fig. S5†) where a decrease in effective surface charge of nanoparticles was observed upon U(VI) adsorption at pH values above 6.

2.2. Equilibrium adsorption experiments

For evaluating U(VI) sorption capacity, adsorption isotherms were obtained for rhamnolipid-coated nanoparticles (Fig. 4) under a variety of conditions. The calculated sorption capacities for different carbonate and pH conditions are shown in Table 1. For open (atmosphere) system conditions, the maximum sorption capacity (q_{max}) decreased significantly as the pH increased from 6 to 8. At pH 6, positively charged species such as UO_2^{2+}, $(UO_2)_2(OH)_2^{2+}$, UO_2OH^+ and $(UO_2)_3(OH)_5^+$ favor adsorption of U(VI) to negatively charged (Fig. 4) rhamnolipid-coated nanoparticles due to electrostatic interactions. However, at pH 8, the sorption capacity was lower owing to the formation of negatively charged stable U(VI) carbonate complexes ($(UO_2(CO_3)_3)^{4-}$, $UO_2(CO_3)_2^{2-}$ and $(UO_2)_2CO_3(OH)_3^-$) that do not adsorb to surfaces and that effectively lower the activity of UO_2^{2+}. Even at pH 6, the adsorption capacity for open to atmosphere conditions is less (116 μg mg^{-1}) than in the carbonate-free system (155 μg mg^{-1}) due to the formation of negatively charged stable uranyl carbonate complexes. For the carbonate-free system, at pH 8, the activity of UO_2^{2+} is much higher as compared to in the open to the atmosphere conditions, which resulted in the favorable adsorption of U(VI) to rhamnolipid-coated IONPs. In addition to the surface complexation models' ability to fit the data (discussed below), both Langmuir and Freundlich models were also fitted to experimental data. The plots in Fig. 4 show that the Langmuir model provides a better fit to the data under all conditions.

The adsorption of U(VI) on rhamnolipid-coated nanoparticles was observed over the range of pH values from 5.5 to 11.5 at two different loadings (1 μM and 10 μM) and three different carbonate conditions (carbonate-free, open to atmosphere, fixed DIC) in 0.01 M $NaNO_3$ (shown in Fig. 5). The two U(VI) loadings were selected as they were below the

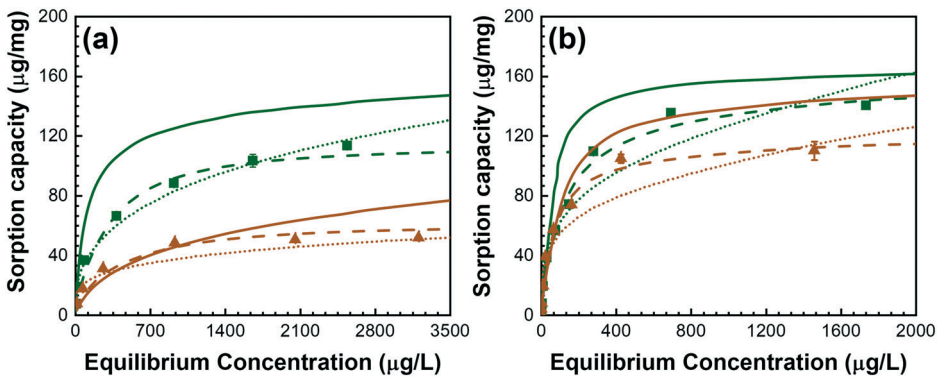

Fig. 4 Adsorption isotherm at pH = 6 and pH = 8 in (a) open to atmosphere conditions and (b) carbonate-free system. ▲ represent points obtained at pH = 8 and ■ represent data points obtained at pH = 6. Dashed lines show the Langmuir fitting and dotted lines represent the Freundlich fitting. DLM parameters were also fitted to the isotherm data and solid lines represent DLM fitting at pH 6 and pH 8.

Table 1 Coefficients for Langmuir and Freundlich models obtained through adsorption isotherm studies

		Langmuir		Freundlich	
Condition	pH	q_{max} ($\mu g\ mg^{-1}$)	K ($L\ \mu g^{-1}$)	K ($(\mu g\ g^{-1})$ $(L\ \mu g^{-1})^{1/n}$)	n
Open to atmosphere	6	116	0.0045	8.61	2.99
	8	52	0.0071	8.03	4.35
Carbonate free system	6	155	0.0080	14.70	3.16
	8	118	0.0154	16.00	3.68

values at which precipitation of uranyl species might occur. The adsorption edges obtained for each set of conditions are shown in Fig. 5.

For the carbonate free system, both 1 μM and 10 μM loadings showed almost 100% sorption until pH ~ 10. At pH >10, sorption efficiency reduced dramatically owing to the steep decrease in UO_2^{2+} availability (shown in ESI,† Fig. S1) in the system. The favorable adsorption at pH values down to pH 5.5 can also be attributed to the presence of positively charged aqueous species that favor adsorption to the negatively charged adsorbent through electrostatic interactions (Fig. S2†).

For adsorption studies with the suspensions equilibrated with the atmosphere, the fraction of total U(VI) adsorbed decreased when loading was increased from 1 μM to 10 μM (Fig. 5). For both loadings adsorption onto IONPs decreased as pH increased above pH 7 due to the formation of stable U(VI) carbonate complexes that lowered the available UO_2^{2+} in the system.

Adsorption edges obtained at 1 mM fixed DIC conditions followed the same trend observed in open to atmosphere conditions with the adsorption percentage decreasing dramatically at higher pH values for the reasons discussed above. However, at lower pH values (<8), the fixed DIC system showed lower adsorption percentages as compared to the open to atmosphere conditions due to less availability of UO_2^{2+} in the fixed DIC system (as shown in Fig. S1†). At pH >8, the trend reversed, owing to more availability of UO_2^{2+} in the fixed DIC system because the supply of CO_3^{2-} for complexing UO_2^{2+} was limited in the fixed DIC system while it continued to increase with increasing pH in the system that was open to uptake of CO_2 from the atmosphere.

Although there is theoretically the possibility of U(VI) reduction to U(IV) due to interaction with Fe(II) in the magnetite nanoparticles, this will only happen if U(VI) diffuses through the rhamnolipid coating. At low U(VI) loadings, as in this case, U(VI) will adsorb on the outer layer before it has a chance to diffuse through the layer to where it could contact the magnetite surface. The absence of dissolved Fe in the supernatant obtained after ultracentrifugation in adsorption studies confirmed that the leaching of iron from rhamnolipid-coated magnetite nanoparticles did not occur at the experimental conditions studied. As the IONPs were stable under all the experimental conditions considered, it is not expected that there was any opportunity for U(VI) to interact directly with the magnetite nanoparticles. Recent studies on U(VI) using bilayer coated IONPs showed that U(VI) reduction was observed only at much higher U(VI) loadings.[9,19] At these higher loadings, the nanoparticles became destabilized, which resulted in changes in the possible diffusion and contact pathway of U(VI) to the surface of nanoparticles.[9,14,19]

2.3. Interpretation of U(VI) adsorption using surface complexation modeling

A surface complexation model was developed to account for U(VI) adsorption to rhamnolipid-coated IONPs in a reaction-based framework that could account for variation in pH, U(VI) loading, and carbonate condition with a single set of surface complexation reactions. The first step in model development was the determination of nanoparticle surface properties (specific surface area, surface site density and acid–base equilibrium constants). Rhamnolipid-coated nanoparticles can only be neutral or negatively charged as the charge is solely decided by protonation/deprotonation of carboxyl groups in the rhamnolipid structure. The charge and pH-

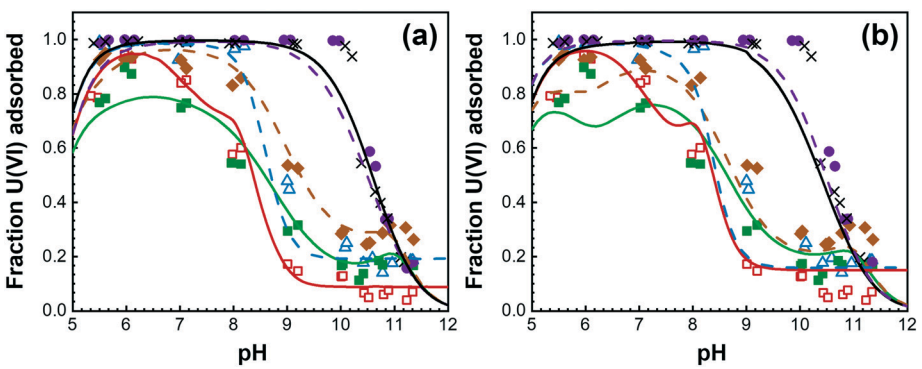

Fig. 5 Comparison of experimental U(VI) adsorption data and output of surface complexation models using (a) the diffuse double layer model (DLM) and (b) a non-electrostatic (NEM) model. The markers represent the experiment data points and lines represent fitting obtained using SCM modeling. X: −10 μM carbonate-free system; ●: −1 μM carbonate-free system; ♦: −1 μM fixed DIC system; ■: −10 μM fixed DIC system; □: −10 μM open to atmosphere and Δ: −1 μM open to atmosphere.

dependence of charge is also evident from zeta potential measurements (Fig. 2). Consequently, the SCM was developed with only protonated (SITEOH) and deprotonated ($SITEO^-$) forms of the surface site.

Potentiometric acid–base titration was performed to determine the surface acidity constant of IONPs. As the pK_a of rhamnolipid lies between 4.3–5.5,[51] rhamnolipid-coated IONPs provided effective buffering from pH 4.5–6.0 (Fig. 2b). The specific surface area was not calculated experimentally as the surface of the magnetite cores of the IONPs may not represent the surface area of the rhamnolipid-coated nanoparticles in aqueous suspension. The optimized values of pK_a, specific surface and site density were determined by minimizing the squares of the residuals between model outputs and experimentally obtained titration curve (Fig. 2b). The best fit was obtained for a specific surface area of 150 $m^2\ g^{-1}$ and site density of 0.73 sites per nm^2. For DLM, the best fit was obtained for a pK_a of 3.6, whereas for NEM the pK_a value obtained was 5.6 (Table 2). The surface site concentration obtained at the optimized values for 30 mg L^{-1} of Fe_3O_4 nanoparticles using optimized values from the titration curve was 22.4 μM. This site concentration value is close to the value of 20.16 μM obtained using TOC analysis. The optimized parameters were used for fitting the adsorption edge and adsorption isotherm data. The obtained surface characteristics were also used to fit the zeta potential measurements obtained using DLS. The Gouy–Chapman equation was used to obtain the surface potential of nanoparticles as a function of pH as shown in Fig. 2a. The model was able to capture the trend of zeta-potential measurements. Zeta potential value is the value obtained on the imaginary slipping plane (where particles interact with each other or other entities), which is less than the actual surface potential of the nanoparticles.[53]

Based on the nanoparticle properties obtained above, DLM was fitted to adsorption edge data (Fig. 4a) obtained at U(VI) loadings of 1 μM and 10 μM and for three sets of carbonate conditions. The best-fitting was obtained using the set of surface complexation reactions shown in Table 2. Aqueous reactions were set at values from a critically-reviewed database (Table S2 in ESI†). In addition to the surface deprotonation reaction (reaction 1) discussed previously, four additional reactions (reactions 2–5) were included for UO_2^{2+} binding to the rhamnolipid carboxyl groups on the IONPs. The $\log K$ values were obtained using MINFIT, which interacts with MINEQL+ to optimize equilibrium constants by minimizing the residual sum of squares between experimental and modeled data.[50]

Reactions 2 and 3 were first used to fit the carbonate-free system, and their $\log K$ values were estimated. Reaction 4 was then added to reactions 2–3 to model the systems with fixed DIC and open to the atmosphere. Various combinations of just two of the reactions in the set that included reactions 2–4 were attempted for fitting, but none of these provided as good of a fit as that provided with all three present, especially for fixed DIC conditions. Consequently, the combination of reactions 2–4 was selected and optimized $\log K$ values for each reaction were obtained using MINFIT. The addition of reaction 4 provided a good fit for carbonate-containing systems at pH values <8, but it underestimated the adsorption percentages at higher pH values. This necessitated the inclusion of another surface complexation reaction that could better describe the fixed DIC and open to atmosphere systems at higher pH values. Reaction 5 was added to the earlier set of reactions and an optimum set of constants was obtained. The inclusion of reaction 5 in the set of reactions reduced the residual sum of squares between experimental data and modelled data by 50%.

NEM was also fitted to adsorption edge data following the same approach used for DLM fitting (Fig. 5b). The model was able to describe the carbonate-free system, but it was not able to capture all the features of the systems with dissolved inorganic carbon. The model was also not able to differentiate between the difference in adsorption percentages obtained at different U(VI) loadings, which was prominent in DLM. The main reason for this was that NEM does not consider the change in surface characteristics of the adsorbent (*e.g.*, change in surface charge) as those are altered by adsorption.

The developed models (DLM and NEM) were also used to fit the adsorption isotherms. The results obtained for the DLM model are shown in Fig. 4, and the fitting obtained for NEM model is shown in ESI† in Fig. S4. The developed SCM models, NEM and DLM, were able to describe the trends observed for both open to atmosphere and carbonate-free systems; however, the maximum sorption capacities were overpredicted by the models. The overprediction may be attributed to bidentate inner-sphere complexation of UO_2^{2+} with rhamnolipid moieties. The actual mode of UO_2^{2+} adsorption to the rhamnolipid-coated IONPs may involve binding to two rhamnolipid functional groups, which would result in a decrease of the maximum sorption capacity of U(VI). Earlier studies on U(VI) sorption to mineral surfaces suggest that both monodentate and bidentate surface complexes are favorable under different pH and carbonate conditions.[3,45,54]

Table 2 Reactions and parameters for diffuse double layer (DLM) and non-electrostatic model (NE)

	Reactions	DLM $\log K$	NEM
1	$SITEOH = SITEO^- + H^+$	−3.60	−5.60
2	$UO_2^{2+} + H_2O + SITEOH = SITEOUO_2OH + 2H^+$	−4.45	−4.12
3	$UO_2^{2+} + 2H_2O + SITEOH = SITEOUO_2OH_2^- + 3H^+$	−8.55	−10.55
4	$UO_2^{2+} + 2CO_3^{2-} + SITEOH = SITEOUO_2(CO_3)_2^{3-} + H^+$	24.60	18.00
5	$UO_2^{2+} + 3CO_3^{2-} + SITEOH = SITEOUO_2(CO_3)_3^{5-} + H^+$	33.50	19.80

3. Conclusions

Based on the optimized particle systems described here, rhamnolipid is a highly effective, biocompatible coating for

stabilizing engineered iron oxide nanoparticles. The use of naturally occurring biosurfactant coatings may be developed as an environmentally benign and cost-effective way for stabilizing nanoparticles in water. The data also show that rhamnolipid-coated nanoparticles act as strong sorbents for U(VI) and can be used for its removal from water over a broad range of water chemistries. The set of four reactions included in SCM were able to predict the adsorption behavior of U(VI) over a wide range of pH and at three different carbonate conditions and two total U(VI) loadings. Excellent agreement between experimental and SCM-predicted sorption values indicate that both electrostatic and chemical interactions are important to U(VI) removal using rhamnolipid-coated IONPs. While these results are promising, further research is needed to systematically investigate the efficiency of these rhamnolipid-coated nanoparticles in real water systems. There is also a need to explore the efficacy of other biosurfactants for the stabilization of these and similar nanoparticles being considered for treatment processes, among other aqueous-based technologies.

Conflicts of interest

There are no conflicts to declare.

Acknowledgements

TEM, DLS, ultracentrifugation, ICP-OES, TOC and ICP-MS measurements were performed in the Nano Research Facility (NRF) at Washington University in St. Louis. We thank the McDonnell International Scholars Academy for their funding to support Neha Sharma in her graduate program. We appreciate the comments of two anonymous reviewers that helped us improve the presentation of our study. Anushree Ghosh is supported by the U.S. National Science Foundation (CBET 1704326), which also supported selected instrumental analysis and materials (CHE 1709484).

References

1 M. Gavrilescu, L. V. Pavel and I. Cretescu, Characterization and remediation of soils contaminated with uranium, *J. Hazard. Mater.*, 2009, **163**, 475–510.
2 C. Tournassat, R. M. Tinnacher, S. Grangeon and J. A. Davis, Modeling uranium(VI) adsorption onto montmorillonite under varying carbonate concentrations: A surface complexation model accounting for the spillover effect on surface potential, *Geochim. Cosmochim. Acta*, 2018, **220**, 291–308.
3 Z. Wang, S. W. Lee, J. G. Catalano, J. S. Lezama-Pacheco, J. R. Bargar, B. M. Tebo and D. E. Giammar, Adsorption of uranium(VI) to manganese oxides: X-ray absorption spectroscopy and surface complexation modeling, *Environ. Sci. Technol.*, 2013, **47**, 850–858.
4 X. Huang, X. Hou, X. Zhang, K. M. Rosso and L. Zhang, Facet-dependent contaminant removal properties of hematite nanocrystals and their environmental implications, *Environ. Sci.: Nano*, 2018, **5**, 1790–1806.
5 X. Guo, R. Chen, Q. Liu, J. Liu, H. Zhang, J. Yu, R. Li, M. Zhang and J. Wang, Superhydrophilic phosphate and amide functionalized magnetic adsorbent: A new combination of anti-biofouling and uranium extraction from seawater, *Environ. Sci.: Nano*, 2018, **5**, 2346–2356.
6 A. S. Helal, E. Mazario, A. Mayoral, P. Decorse, R. Losno, C. Lion, S. Ammar and M. Hémadi, Highly efficient and selective extraction of uranium from aqueous solution using a magnetic device: Succinyl-β-cyclodextrin-APTES@maghemite nanoparticles, *Environ. Sci.: Nano*, 2018, **5**, 158–168.
7 X. Huang, X. Hou, F. Wang, B. Guo, F. Song, L. Ling, J. Zhao and L. Zhang, Molecular-scale structures of uranyl surface complexes on hematite facets, *Environ. Sci.: Nano*, 2019, **6**, 892–903.
8 T. Wan, W. Cheng, J. Ren, W. Wu, M. Wang, B. Hu, Z. Jia and Y. Sun, The influence of nanoscale size on the adsorption-desorption of U(vi) on nano-Al oxides, *Environ. Sci.: Nano*, 2018, **5**, 2731–2741.
9 W. Li, J. T. Mayo, D. N. Benoit, L. D. Troyer, Z. A. Lewicka, B. J. Lafferty, J. G. Catalano, S. S. Lee, V. L. Colvin and J. D. Fortner, Engineered superparamagnetic iron oxide nanoparticles for ultra-enhanced uranium separation and sensing, *J. Mater. Chem. A*, 2016, **4**, 15022–15029.
10 A. A. Alqadami, M. Naushad, Z. A. Alothman and A. A. Ghfar, Novel Metal-Organic Framework (MOF) Based Composite Material for the Sequestration of U(VI) and Th(IV) Metal Ions from Aqueous Environment, *ACS Appl. Mater. Interfaces*, 2017, **9**, 36026–36037.
11 D. Das, M. K. Sureshkumar, S. Koley, N. Mithal and C. G. S. Pillai, Sorption of uranium on magnetite nanoparticles, *J. Radioanal. Nucl. Chem.*, 2010, **285**, 447–454.
12 S. S. Lee, W. Li, C. Kim, M. Cho, J. G. Catalano, B. J. Lafferty, P. Decuzzi and J. D. Fortner, Engineered manganese oxide nanocrystals for enhanced uranyl sorption and separation, *Environ. Sci.: Nano*, 2015, **2**, 500–508.
13 M. Tang, J. Chen, P. Wang, C. Wang and Y. Ao, Highly efficient adsorption of uranium(vi) from aqueous solution by a novel adsorbent: Titanium phosphate nanotubes, *Environ. Sci.: Nano*, 2018, **5**, 2304–2314.
14 Z. Pan, W. Li, J. D. Fortner and D. E. Giammar, Measurement and Surface Complexation Modeling of U(VI) Adsorption to Engineered Iron Oxide Nanoparticles, *Environ. Sci. Technol.*, 2017, **51**, 9219–9226.
15 M. Wazne, X. Meng, G. P. Korfiatis and C. Christodoulatos, Carbonate effects on hexavalent uranium removal from water by nanocrystalline titanium dioxide, *J. Hazard. Mater.*, 2006, **136**, 47–52.
16 R. De Palma, S. Peeters, M. J. Van Bael, H. Van Den Rul, K. Bonroy, W. Laureyn, J. Mullens, G. Borghs and G. Maes, Silane ligand exchange to make hydrophobic superparamagnetic nanoparticles water-dispersible, *Chem. Mater.*, 2007, **19**, 1821–1831.
17 S. Laurent, D. Forge, M. Port, A. Roch, C. Robic, L. Vander Elst and R. N. Muller, Magnetic Iron Oxide Nanoparticles: Synthesis, Stabilization, Vectorization, Physicochemical

Characterizations, and Biological Applications, *Chem. Rev.*, 2008, **108**, 2064–2110.

18 W. Jiang, Q. Cai, W. Xu, M. Yang, Y. Cai, D. D. Dionysiou and K. E. O'Shea, Cr(VI) adsorption and reduction by humic acid coated on magnetite, *Environ. Sci. Technol.*, 2014, **48**, 8078–8085.

19 W. Li, L. D. Troyer, S. S. Lee, J. Wu, C. Kim, B. J. Lafferty, J. G. Catalano and J. D. Fortner, Engineering Nanoscale Iron Oxides for Uranyl Sorption and Separation: Optimization of Particle Core Size and Bilayer Surface Coatings, *ACS Appl. Mater. Interfaces*, 2017, **9**, 13163–13172.

20 W. Li, S. S. Lee, J. Wu, C. H. Hinton and J. D. Fortner, Shape and size controlled synthesis of uniform iron oxide nanocrystals through new non-hydrolytic routes, *Nanotechnology*, 2016, **27**, 324002.

21 M. Basnet, S. Ghoshal and N. Tufenkji, Rhamnolipid biosurfactant and soy protein act as effective stabilizers in the aggregation and transport of palladium-doped zerovalent iron nanoparticles in saturated porous media, *Environ. Sci. Technol.*, 2013, **47**, 13355–13364.

22 W. Li, C. H. Hinton, S. S. Lee, J. Wu and J. D. Fortner, Surface engineering superparamagnetic nanoparticles for aqueous applications: Design and characterization of tailored organic bilayers, *Environ. Sci.: Nano*, 2016, **3**, 85–93.

23 S. Ge, M. Agbakpe, Z. Wu, L. Kuang, W. Zhang and X. Wang, Influences of surface coating, UV irradiation and magnetic field on the algae removal using magnetite nanoparticles, *Environ. Sci. Technol.*, 2015, **49**, 1190–1196.

24 V. Patsula, L. Kosinová, M. Lovrić, L. Ferhatovic Hamzić, M. Rabyk, R. Konefal, A. Paruzel, M. Šlouf, V. Herynek, S. Gajović and D. Horák, Superparamagnetic Fe3O4 Nanoparticles: Synthesis by Thermal Decomposition of Iron(III) Glucuronate and Application in Magnetic Resonance Imaging, *ACS Appl. Mater. Interfaces*, 2016, **8**, 7238–7247.

25 G. Luongo, P. Campagnolo, J. E. Perez, J. Kosel, T. K. Georgiou, A. Regoutz, D. J. Payne, M. M. Stevens, M. P. Ryan, A. E. Porter and I. E. Dunlop, Scalable High-Affinity Stabilization of Magnetic Iron Oxide Nanostructures by a Biocompatible Antifouling Homopolymer, *ACS Appl. Mater. Interfaces*, 2017, **9**, 40059–40069.

26 C. Kim, S. S. Lee, B. J. Lafferty, D. E. Giammar and J. D. Fortner, Engineered superparamagnetic nanomaterials for arsenic(v) and chromium(VI) sorption and separation: Quantifying the role of organic surface coatings, *Environ. Sci.: Nano*, 2018, **5**, 556–563.

27 Y. Xie, R. Ye and H. Liu, Synthesis of silver nanoparticles in reverse micelles stabilized by natural biosurfactant, *Colloids Surf., A*, 2006, **279**, 175–178.

28 A. Szymanska and Z. Sadowski, Effects of biosurfactants on surface properties of hematite, *Adsorption*, 2010, **16**, 233–239.

29 C. N. Mulligan, Recent advances in the environmental applications of biosurfactants, *Curr. Opin. Colloid Interface Sci.*, 2009, **14**, 372–378.

30 S. Bhattacharjee, M. Basnet, N. Tufenkji and S. Ghoshal, Effects of Rhamnolipid and Carboxymethylcellulose Coatings on Reactivity of Palladium-Doped Nanoscale Zerovalent Iron Particles, *Environ. Sci. Technol.*, 2016, **50**, 1812–1820.

31 C. A. Marangon, V. C. A. Martins, M. H. Ling, C. C. Melo, A. M. G. Plepis, R. L. Meyer and M. Nitschke, Combination of Rhamnolipid and Chitosan in Nanoparticles Boosts Their Antimicrobial Efficacy, *ACS Appl. Mater. Interfaces*, 2020, **12**, 5488–5499.

32 G. Balakrishnan, M. Déniel, T. Nicolai, C. Chassenieux and F. Lagarde, Towards more realistic reference microplastics and nanoplastics: preparation of polyethylene micro/nanoparticles with a biosurfactant, *Environ. Sci.: Nano*, 2019, **6**, 315–324.

33 G. Huang, W. Peng and S. Yang, Synthesis of magnetic chitosan/graphene oxide nanocomposites and its application for U(VI) adsorption from aqueous solution, *J. Radioanal. Nucl. Chem.*, 2018, **317**, 337–344.

34 Y. Cai, C. Wu, Z. Liu, L. Zhang, L. Chen, J. Wang, X. Wang, S. Yang and S. Wang, Fabrication of a phosphorylated graphene oxide-chitosan composite for highly effective and selective capture of U(VI), *Environ. Sci.: Nano*, 2017, **4**, 1876–1886.

35 S. Wang and C. N. Mulligan, Rhamnolipid biosurfactant-enhanced soil flushing for the removal of arsenic and heavy metals from mine tailings, *Process Biochem.*, 2009, **44**, 296–301.

36 S. De, S. Malik, A. Ghosh, R. Saha and B. Saha, A review on natural surfactants, *RSC Adv.*, 2015, **5**, 65757–65767.

37 P. Singh, S. Ravindran, J. K. Suthar, P. Deshpande, R. Rokhade and V. Rale, Production of biosurfactant stabilized nanoparticles, *Int. J. Pharm. Biol. Sci.*, 2017, **8**, 701–707.

38 M. Basnet, A. Gershanov, K. J. Wilkinson, S. Ghoshal and N. Tufenkji, Interaction between palladium-doped zerovalent iron nanoparticles and biofilm in granular porous media: Characterization, transport and viability, *Environ. Sci.: Nano*, 2016, **3**, 127–137.

39 X. Zhao, W. Liu, Z. Cai, B. Han, T. Qian and D. Zhao, An overview of preparation and applications of stabilized zero-valent iron nanoparticles for soil and groundwater remediation, *Water Res.*, 2016, **100**, 245–266.

40 B. N. Singh, A. K. S. Rawat, W. Khan, A. H. Naqvi and B. R. Singh, Biosynthesis of stable antioxidant ZnO nanoparticles by Pseudomonas aeruginosa Rhamnolipids, *PLoS One*, 2014, **9**, DOI: 10.1371/journal.pone.0106937.

41 C. Hazra, D. Kundu, A. Chaudhari and T. Jana, Biogenic synthesis, characterization, toxicity and photocatalysis of zinc sulfide nanoparticles using rhamnolipids from Pseudomonas aeruginosa BS01 as capping and stabilizing agent, *J. Chem. Technol. Biotechnol.*, 2013, **88**, 1039–1048.

42 Z. Hosseinidoust, M. Basnet, T. G. M. Van De Ven and N. Tufenkji, One-pot green synthesis of anisotropic silver nanoparticles, *Environ. Sci.: Nano*, 2016, **3**, 1259–1264.

43 M. O. Barnett, P. M. Jardine and S. C. Brooks, U(VI) adsorption to heterogeneous subsurface media: Application of a surface complexation model, *Environ. Sci. Technol.*, 2002, **36**, 937–942.

44 L. Qian, M. Ma and D. Cheng, Adsorption and desorption of uranium on nano goethite and nano alumina, *J. Radioanal. Nucl. Chem.*, 2015, **303**, 161–170.

45 H. Zeng, A. Singh, S. Basak, K. U. Ulrich, M. Sahu, P. Biswas, J. G. Catalano and D. E. Giammar, Nanoscale size effects on uranium(VI) adsorption to hematite, *Environ. Sci. Technol.*, 2009, **43**, 1373–1378.

46 M. I. Boyanov, E. J. O'Loughlin, E. E. Roden, J. B. Fein and K. M. Kemner, Adsorption of Fe(II) and U(VI) to carboxyl-functionalized microspheres: The influence of speciation on uranyl reduction studied by titration and XAFS, *Geochim. Cosmochim. Acta*, 2007, **71**, 1898–1912.

47 T. A. Duster, J. E. S. Szymanowski and J. B. Fein, Experimental Measurements and Surface Complexation Modeling of U(VI) Adsorption onto Multilayered Graphene Oxide: The Importance of Adsorbate-Adsorbent Ratios, *Environ. Sci. Technol.*, 2017, **51**, 8510–8518.

48 K. L. Chen, S. E. Mylon and M. Elimelech, Aggregation kinetics of alginate-coated hematite nanoparticles in monovalent and divalent electrolytes, *Environ. Sci. Technol.*, 2006, **40**, 1516–1523.

49 T. D. Waite, J. A. Davis, T. E. Payne, G. A. Waychunas and N. Xv, U(VI) Adsorption to Ferrihydrite: Application of a Surface Complexation Model, *Geochim. Cosmochim. Acta*, 1994, **58**, 5465–5478.

50 X. Xie, D. E. Giammar and Z. Wang, MINFIT: A Spreadsheet-Based Tool for Parameter Estimation in an Equilibrium Speciation Software Program, *Environ. Sci. Technol.*, 2016, **50**, 11112–11120.

51 A. Lebrón-Paler, J. E. Pemberton, B. A. Becker, W. H. Otto, C. K. Larive and R. M. Maier, Determination of the acid dissociation constant of the biosurfactant monorhamnolipid in aqueous solution by potentiometric and spectroscopic methods, *Anal. Chem.*, 2006, **78**, 7649–7658.

52 W. W. Yu, J. C. Falkner, C. T. Yavuz and V. L. Colvin, Synthesis of monodisperse iron oxide nanocrystals by thermal, *Chem. Commun.*, 2004, 2306–2307.

53 G. V. Lowry, R. J. Hill, S. Harper, A. F. Rawle, C. O. Hendren, F. Klaessig, U. Nobbmann, P. Sayre and J. Rumble, Guidance to improve the scientific value of zeta-potential measurements in nanoEHS, *Environ. Sci.: Nano*, 2016, **3**, 953–965.

54 J. H. Jang, B. A. Dempsey and W. D. Burgos, A model-based evaluation of sorptive reactivities of hydrous ferric oxide and hematite for U(VI), *Environ. Sci. Technol.*, 2007, **41**, 4305–4310.

